

First Principles Study of Angular Dependence of Spin-Orbit Torque in Pt/Co and Pd/Co Bilayers

Farzad Mahfouzi^{1,*} and Nicholas Kioussis^{1,†}

¹*Department of Physics and Astronomy, California State University, Northridge, CA, USA*

Spin-orbit torque (SOT) induced by spin Hall and interfacial effects in heavy metal(HM)/ferromagnetic(FM) bilayers has recently been employed to switch the magnetization direction using in-plane current injection. In this paper, using the Keldysh Green's function approach and first principles electronic structure calculations we determine the Field-Like (FL) and Damping-Like (DL) components of the SOT for the HM/Co (HM = Pt, Pd) bilayers. Our approach yields the angular dependence of both the FL- and DL-SOT on the magnetization direction without assuming a priori their angular form. Decomposition of the SOT into the Fermi sea and Fermi surface contributions reveals that the SOT is dominated by the latter. Due to the large lattice mismatch between the Co and the HM we have also determined the effect of tensile biaxial strain on both the FL- and DL-SOT components. The calculated dependence of FL- and DL-SOT on the HM thickness is overall in good agreement with experiment. The dependence of the SOT with the position of the Fermi level suggests that the DL-SOT dominated by the Spin Hall effect of the bulk HM.

PACS numbers: 72.25.Mk, 75.70.Tj, 85.75.-d, 72.10.Bg

I. INTRODUCTION

Spin-Orbit Torque (SOT) due to inplane current flow in heavy-metal/ferromagnet (HM/FM) bilayers has attracted considerable attention in recent years as a method to switch efficiently the magnetization direction of ultrathin FM films at room temperature.^{1–7} Experimental^{2,5,7,8} and theoretical^{9–11} studies have established that the SOT can be separated into a Field-Like (FL), $T^{FL}\vec{m} \times \vec{y}$, and Damping-Like (DL), $T^{DL}\vec{m} \times (\vec{m} \times \vec{y})$, components, where \vec{m} is the unit vector pointing along the direction of the magnetization and \vec{y} is an in-plane unit vector normal to the applied electric field. In the linear response regime, the FL-SOT changes both the size and direction of the effective magnetic field, while the DL-SOT only reorients the effective field and is responsible for the angular momentum transfer between the flowing electrons and the FM, thus modulating the ferromagnetic resonance linewidth of the FM^{12–14}.

Experimentally, different techniques including, the adiabatic (low-frequency) harmonic Hall voltage^{15–18}, the Spin-Torque Ferromagnetic Resonance(ST-FMR)^{18–22} and the magneto-optical Kerr effect (MOKE)^{23,24}, have been used to quantitatively measure the DL- and FL-SOT components. Furthermore, the adiabatic harmonic Hall voltage approach has been recently employed to investigate the magnetization orientation dependence of the SOT^{17,25,26}.

The experimental observations invite several important questions pertaining to the microscopic origin of: (i) The bulk versus interfacial SOT^{9,11,27,28} (ii) Higher order angular terms of the FL-SOT^{8,17,25,26} and (iii) The HM thickness dependence of the SOT^{17,29}. To address these questions an accurate description of the electronic structure of the bilayer in terms of the crystal structure and the interfacial hybridization of the electron orbitals

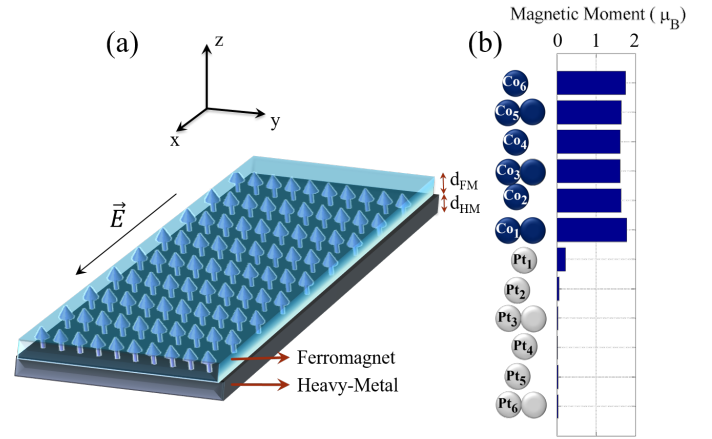


FIG. 1: (Color online) (a) Schematic device setup consisting of a Ferromagnet/Heavy-Metal bilayer system under an applied electric field along the x -axis. (b) Atomic stacking along the $[111]$ direction of the Co/Pt bilayer slab composed of six layers of hcp Co on six layers of fcc Pt (111). We also show the layer-resolved magnetic moment.

is necessary.

The objective of this work is to employ an *ab initio*-based framework which links the Keldysh Green's function approach with first principles electronic structure calculations to determine the FL- and DL-SOT of the Co/Pt and Co/Pd (111) bilayers. This approach yields the well-known angular forms for both SOT components without assuming a priori their angular dependence. We show that the DL-SOT can be separated into Fermi sea and Fermi surface contributions where the latter is dominant. We present results of the effect of biaxial strain and of heavy metal thickness on both components of the SOT and compare the *ab initio* results with experiment.

In agreement with experiment, we find that the FL-SOT saturates with decreasing HM thickness indicating its interfacial origin due to the Rashba-Edelstein effect (REE). On the other hand, the DL-SOT vanishes with decreasing HM thickness suggesting its bulk origin due to the Spin Hall Effect (SHE). This is corroborated by the strong correlation of the dependence of the DL-SOT and SHC on the Fermi level position of the heavy metal.

II. THEORETICAL FORMALISM

The magnetization dynamics of a FM described by a time-dependent unit vector, \vec{m} , along the magnetization orientation, is described by the Landau-Lifshitz-Gilbert (LLG) equation of motion,

$$\frac{d\vec{m}}{dt} = -\vec{m} \times \gamma \vec{H}_{ext} + \vec{T} + \alpha \vec{m} \times \frac{d\vec{m}}{dt}. \quad (1)$$

Here, γ is the gyromagnetic ratio, α is the Gilbert damping constant, \vec{H}_{ext} is the external magnetic field and \vec{T} , is the current-induced torque on the FM which can be written in the form,

$$\vec{T} = \frac{1}{N_k M_s} \vec{m} \times \sum_{\vec{k}} \text{Tr} \left(\frac{\partial \hat{H}_{\vec{k}}}{\partial \vec{m}} \hat{\rho}_{\vec{k}} \right), \quad (2)$$

where, N_k is the number of k -point mesh for the numerical integration, M_s is the magnetic moment per unit cell in units of Bohr magneton, μ_B , $\hat{H}_{\vec{k}}(\vec{m})$ is the electronic Hamiltonian which depends on \vec{m} and $\hat{\rho}_{\vec{k}}$ is the electronic density matrix.

In the absence of an external electric field or a time-dependent term in the Hamiltonian, the electronic density matrix is given by $\hat{\rho}_{\vec{k}}^{eq} = \int dE \text{Im}(\hat{G}_{\vec{k}E}) f(E) / \pi$, where, $\hat{G}_{\vec{k}E} = (E - i\eta - \hat{H}_{\vec{k}})^{-1}$ is the electron Green's function and $f(E)$ is the Fermi distribution function. Here, $\eta = \hbar/2\tau$ is the broadening parameter, where τ is the relaxation time for the excited electrons. Typically, \vec{T}^{eq} contributes to the exchange interaction between local moments and is responsible for the magnetocrystalline anisotropy arising from the spin-orbit coupling (SOC). To go beyond the equilibrium regime and investigate the effect of the external electric field on the density matrix we employ the Keldysh Green's function formalism³⁰, where the density matrix is given by, $\hat{\rho}_{\vec{k}} = \eta \int dE \hat{G}_{\vec{k}E} f(E) \hat{G}_{\vec{k}E}^\dagger / \pi$. In the presence of an external electric field, \vec{E}_{ext} the energy in the integrand is replaced with $E \rightarrow E + ie\vec{E}_{ext} \cdot \nabla_{\vec{k}}$. In the linear response regime the nonequilibrium density matrix of the electrons under an external electric field along the x direction is

$$\frac{\hat{\rho}_{\vec{k}}^{neq}}{eE_{ext}^x} = \hbar \int \frac{dE}{2\pi i} \left[\text{Im} \left(\hat{G}_{\vec{k}E} \frac{\partial \hat{G}_{\vec{k}E}}{\partial k_x} - \frac{\partial \hat{G}_{\vec{k}E}}{\partial k_x} \hat{G}_{\vec{k}E} \right) f(E) - \eta \left(\hat{G}_{\vec{k}E} \frac{\partial \hat{G}_{\vec{k}E}^\dagger}{\partial k_x} - \frac{\partial \hat{G}_{\vec{k}E}}{\partial k_x} \hat{G}_{\vec{k}E}^\dagger \right) \frac{\partial f(E)}{\partial E} \right]. \quad (3)$$

The first term in the integrand is the Fermi sea contribution originating from the modification of the single electron Green's function due to the electric field and the second term is the Fermi surface contribution. Using the Fermi Surface (FS) contribution of the nonequilibrium density matrix in Eq. (2) the FS contribution to the current-induced SOT torkance, $\vec{\tau}_{FS} = \vec{T}_{FS}^{neq} / eE_{ext}^x$, is given by

$$\vec{\tau}_{FS} = \frac{1}{\pi M_s N_k} \vec{m} \times \sum_{\vec{k}} \text{Im} \left(\text{Tr} \left[\frac{\partial \hat{H}_{\vec{k}}}{\partial \vec{m}} \text{Im}(\hat{G}_{\vec{k}}) \hat{v}_{k_x} \hat{G}_{\vec{k}} \right] \right). \quad (4)$$

Here, $\hat{v}_{k_x} = \frac{\partial \hat{H}_{\vec{k}}}{\partial k_x}$ is the group velocity matrix and the Green's functions are calculated at the Fermi energy, $E = E_F$. The torkance can be separated into the field-like ($\vec{\tau}^{FL}$) and a damping-like ($\vec{\tau}^{DL}$) components corresponding to the imaginary and real parts of the Green's function, $\hat{G}_{\vec{k}} = \text{Re}(\hat{G}_{\vec{k}}) + i\text{Im}(\hat{G}_{\vec{k}})$, respectively. Note that $\vec{\tau}^{FL}$ ($\vec{\tau}^{DL}$) is even (odd) under $\eta \rightarrow -\eta$ transformation. A similar decomposition can also be made from the even and odd components of the torkance under $\vec{m} \rightarrow -\vec{m}$ transformation¹¹.

The total non-equilibrium density matrix given by Eq.(3) can be rewritten in the following form,

$$\frac{\hat{\rho}_{\vec{k}}^{neq}}{eE_{ext}^x} = \hbar \int \frac{dE}{\pi} \left[\text{Im}(\hat{G}_{\vec{k}E}) \hat{v}_{k_x} \text{Im}(\hat{G}_{\vec{k}E}) \frac{\partial f(E)}{\partial E} - 2\text{Im} \left(\text{Im}(\hat{G}_{\vec{k}E}) \hat{v}_{k_x} \text{Re}(\hat{G}_{\vec{k}E}^2) \right) f(E) \right], \quad (5)$$

where, the first term leads to the FL-SOT and remains to be a FS quantity only, $\tau_{tot}^{FL} = \tau_{FS}^{FL}$. The second term leads to the total DL-SOT, where, in the ballistic regime, $\eta \rightarrow 0$ and in a representation in which the Hamiltonian is diagonal, we can use $\text{Im}(\hat{G}_{\vec{k}E})_{nn} = \pi \delta(E - \varepsilon_n(\vec{k}))$ to obtain,

$$\vec{\tau}_{tot}^{DL} = \frac{2}{M_s N_k} \vec{m} \times \sum_{nm\vec{k}} \text{Re} \left(\frac{\text{Im} \left(\left(\frac{\partial \hat{H}_{\vec{k}}}{\partial \vec{m}} \right)_{nm} \hat{v}_{mn}^{k_x} \right)}{(\varepsilon_{n\vec{k}} - \varepsilon_{m\vec{k}} - i\eta)^2} \right) f(\varepsilon_{n\vec{k}}), \quad (6)$$

where, n and m are band indices and $\varepsilon_{n\vec{k}}$ are the energy bands. Eq. (6) is sometimes rewritten in terms of the Berry curvature^{10,11,31} which unlike the Fermi surface contribution that requires a non-zero density of states at the Fermi surface (*i.e.* due to the presence of $\text{Im}(\hat{G}_{\vec{k}E_F})$), the total DL-SOT can in principle be nonzero even if the system is an insulator, as for example in the case of ferromagnetic/topological insulator heterostructures^{32,33}. In Sec. IV we present results for the both the Fermi sea and Fermi surface contribution to the DL-SOT using Eqs.(4) and (6), respectively.

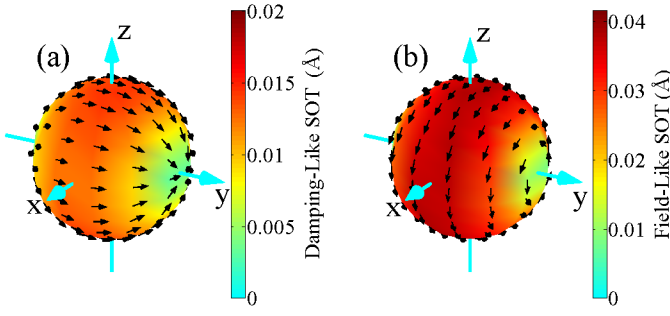


FIG. 2: (Color online) Angular dependence of the total (a) DL-SOT, $\vec{\tau}_{tot}^{DL}$ and (b) FL-SOT, $\vec{\tau}_{tot}^{FL}$, on the magnetization direction, \vec{m} , for the Pt(8 ML)/Co(6 ML) bilayer under an external electric field \vec{E}_{ext} along x and for broadening parameter, $\eta = 28 meV$. The color (arrow) denotes the magnitude (direction) of the SOT for each magnetization direction.

III. DFT CALCULATION

The density functional theory calculations for the hcp Co(0001)/fcc Pt(111) and Co(0001)/fcc Pd(111) bilayers were carried out using the Vienna *ab initio* simulation package (VASP)^{34,35}. The pseudopotential and wave functions are treated within the projector-augmented wave (PAW) method^{36,37}. Structural relaxations were carried using the generalized gradient approximation as parameterized by Perdew *et al.*³⁸ when the largest atomic force is smaller than 0.01 eV/Å. As illustrated in Fig. 1(b), the HM(m)/Co(n) bilayer is modeled employing the slab supercell approach along the [111] consisting of m fcc Pt or Pd monolayers (MLs) with ABC stacking ($m=1, 2, \dots, 8$) and $n=6$ hcp Co MLs with AB stacking. A 25 Å thick vacuum region is introduced to separate the periodic slabs along the stacking direction (*i.e.* z -axis). The plane wave cutoff energy is 500 eV and a $14 \times 14 \times 1$ k points mesh is used in the 2D Brillouin Zone (BZ) sampling. The in-plane lattice constant of the hexagonal unit cell is set to the experimental value of 2.505 Å for bulk Co. Furthermore, in order to investigate the effect of epitaxial strain on the SOT we have varied the in-plane lattice constant in the range of $a \in (2.5, 2.77)$ Å, where the latter value corresponds to the bulk Pt lattice constant. Using the tight-binding Hamiltonian obtained from the VASP-Wannier90 calculations³⁹ as detailed in Ref.⁴⁰, we have calculated the SOT versus magnetization orientation with a $500 \times 500 \times 1$ k point mesh for the BZ sampling.

IV. RESULTS AND DISCUSSION

Figs. 2(a) and (b) show the angular dependence of the $\vec{\tau}_{tot}^{DL}$ and $\vec{\tau}_{tot}^{FL}$ components for the Pt (8 ML)/Co (6 ML) calculated from Eqs. (4) and (6), respectively, with $\eta = 28 meV$. The results show that the angular dependence of the FL-SOT and DL-SOT components

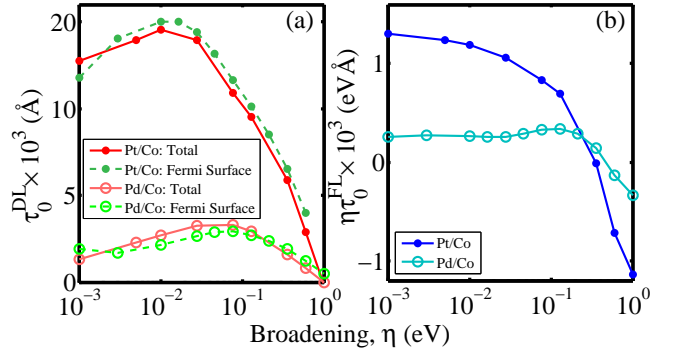


FIG. 3: (Color online) (a) Fermi surface contribution (dashed curves) and total (solid curve) DL-SOT and (b) FL-SOT versus broadening parameter, η for Pt(8 ML)/Co(6 ML) (filled circles) and Pd (8 ML)/Co (6 ML) (open circles) bilayers, respectively. The total and Fermi surface contribution for the DL-SOT were calculated using Eqs. (6) and (4), respectively.

follow the expected $\vec{\tau}^{FL} = \tau_0^{FL}(\hat{y} \times \vec{m})$ and $\vec{\tau}^{DL} = \tau_0^{DL}\vec{m} \times (\hat{y} \times \vec{m})$ behavior, without however, a priori assumption of their angular form. Within the accuracy of the calculations, we do not find any contribution from higher-order angular contributions of the magnetization direction, \vec{m} , to the FL-SOT, as suggested by the experimental observations^{8,17}.

In Figs. 3(a) and (b) we present the FL- and DL-SOT versus the energy broadening parameter, η , for the Pt (8 ML)/Co(6 ML) and Pd (8 ML)/Co(6 ML) bilayer systems, using the in-plane lattice constant, $a=2.5\text{Å}$, of bulk Co. The dashed and solid curves in Fig. 3(a) represent the Fermi surface [Eq. (4)] and total [Eq. (6)] DL-SOT, respectively. The results show that: (i) within the numerical accuracy of the calculations, the DL-SOT originates exclusively from electrons on the Fermi surface; (ii) τ_0^{DL} converges to a finite value as $\eta \rightarrow 0$, while $\tau_0^{FL}(\eta)$ diverges as $1/\eta$ demonstrating their intrinsic and extrinsic characteristics, respectively; and (iii) the DL-SOT exhibits a non-monotonic dependence with η while $\eta\tau_0^{FL}(\eta)$ decreases rather monotonically and changes sign for larger η values.

Since the lattice constant of bulk Pt ($a_{Pt} = 2.8\text{Å}$) and Pd ($a_{Pd} = 2.75\text{Å}$) are larger than that of bulk Co ($a_{Co} = 2.5\text{Å}$), in Figs. 4(a) and (b) we show the strain dependence of the FL- and DL-SOT, respectively, for the Pt(6 ML)/Co(6 ML) and Pd(6 ML)/Co(6 ML), where the strain, $\epsilon = (a - a_{Co})/a_{Co}$, and the broadening parameter, $\eta = 0.13$ eV. The increase of the DL-SOT in Pt/Co (Pd/Co) bilayer can be attributed to the decrease of the electronic group velocity with increasing biaxial inplane tensile strain and a larger increase of the group velocity due to larger concomitant compression of the interlayer distances which lead to an overall increase of the SHC which is proportional to the product of the two group velocities. On the other hand, the FL-SOT increases for the Pt/Co bilayer while it decreases for the Pd/Co bilayer, suggesting the absence of a universal strain dependence

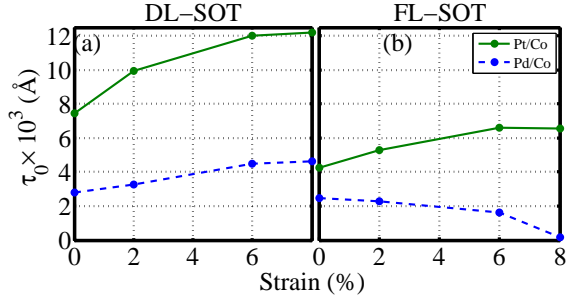


FIG. 4: (Color online) (a) FL-SOT and (b) DL-SOT versus tensile biaxial in-plane strain on the Co, for Pt (6 ML)/Co(6 ML) (solid curves) and Pd (6 ML)/Co(6 ML) (dashed curves), respectively, for $\eta = 0.13$ eV.

of the FL-SOT with biaxial tensile strain.

In order to elucidate the effect of the HM (Pt, Pd) thickness on the SOT we display in Fig. 5 the thickness dependence of the DL- and FL-SOT for $\eta = 0.01$ eV [(a) and (b)] corresponding to a relatively clean system and $\eta = 0.13$ eV [(c) and (d)] for the “diffusive” case within the relaxation time approximation regime. The DL-SOT for the clean system [Fig. 5(a)] exhibits a nonlinear dependence on HM thickness of the form, $\propto 1 - \text{sech}(d_{HM}/\lambda_{HM}) \approx \frac{1}{2} \left(\frac{d_{HM}}{\lambda_{HM}} \right)^2$, for small HM thickness¹⁷. The agreement with the experimental findings for Pd/Co¹⁷ and Pt/Co²⁹ is overall good. The *ab initio* calculations underestimate the DL-SOT for Pt/Co which may be due to the strain effect shown in Fig. 4(a). On the other hand, our DL-SOT results for the Pd/Co bilayer yield a smaller spin diffusion length which can be attributed to the violation of conservation laws within the relaxation time approximation. Consequently, the treatment of systems with relatively weak SOC requires a more accurate mechanism^{40,41} of the spin relaxation. For the Pd/Co bilayer both the increase of the FL-SOT with increasing Pd thickness and its saturation as $d_{Pd} \rightarrow 0$ are consistent with experiment indicating its interfacial origin¹⁷. For the Pt/Co bilayer the FL-SOT reverses sign at 1 ML Pt thickness while experiments report a reversal at about 8 ML (≈ 2 nm)²⁹.

In order to gain an insight into the origin of the SOT and how it changes with shift of the chemical potential, *e.g.* due to doping, in Fig. 6(a) and (b) we present both the FL- and DL-SOT for the Pt(6 ML)/Co(6 ML) and Pd(6 ML)/Co(6 ML) bilayers, respectively, as a function of the Fermi level position, $\mu - E_F$ (E_F is the Fermi level) for $\eta = 0.1$ eV. The FL-SOT in both systems reverses sign as the chemical potential is raised to about +0.1 eV which may be the origin of the experimentally reported sign reversal of the FL-SOT in ultrathin Pt due to electron doping²⁹. To understand the origin of the dependence of the DL-SOT on the Fermi level position in Figs. 6 (c) and (d) we present the spin Hall conductivity (SHC) of bulk Pt and Pd, respectively, versus the shift of the chemical potential. The SHC is calculated

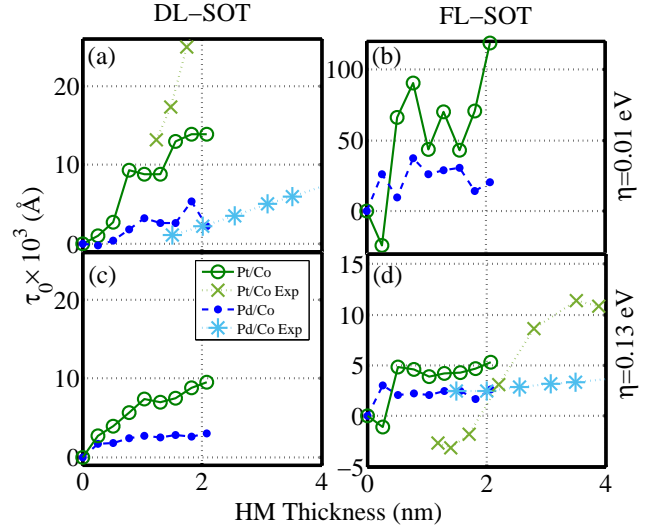


FIG. 5: (Color online) Calculated DL-SOT for Pt(n ML)/Co(6 ML) (green circles) and Pd (n ML)/Co(6 ML) (blue circles) versus the HM layer thickness for η of (a) 0.01 eV (ballistic regime) and (c) 0.13 eV (diffusive regime), respectively. Calculated FL-SOT for Pt(n ML)/Co(6 ML) (green circles) and Pd (n ML)/Co(6 ML) (blue circles) versus the HM layer thickness for η of (b) 0.01 eV and (d) 0.13 eV, respectively. For comparison we also show the experimental DL- and FL-SOT results for the Pt/Co²⁹ and Pd/Co¹⁷ bilayers.

by replacing $\frac{1}{M_s} \vec{m} \times \frac{\partial \hat{H}_{\vec{k}}}{\partial \vec{m}}$ in Eq. (6) with $\frac{e^2}{\hbar^2 V_{HM}} I_z^{S_y}$, where $I_z^{S_y} = \frac{\hbar}{4} \{ \hat{\sigma}^y, \frac{\partial \hat{H}_{\vec{k}}}{\partial k_z} \}$ is the spin current operator and V_{HM} is the volume per unit cell of the HM. Due to the large in-plane lattice constant mismatch between the Pt (Pd) and Co of about -11% (-9%) we also show in Figs. 6 (c) and (d) the SHC of the tetragonally strained bulk Pt and Pd. We find that the biaxial strain results in a reduction of the maximum SHC values and a shift of the SHC peaks to lower energies which can arise from the reduction of the out-of-plane hopping matrix elements due to tensile strain along z . One can clearly see the correlation of the DL-SOT with the SHC over a wide range of chemical potential shift demonstrating that the DL-SOT is dominated by the SHE of the bulk HM.

V. CONCLUDING REMARKS

We have employed an *ab initio*-based framework which links the Keldysh Green’s function approach with first principles electronic structure calculations to determine the FL- and DL-SOT of the Co/Pt and Co/Pd (111) bilayers. Without assuming a priori the angular form of the SOT components, we find that the dependence of the DL-SOT on magnetization direction is of the form $\vec{\tau}_{DL} = \tau_0^{DL} \vec{m} \times (\vec{m} \times \vec{y})$ in agreement with experiment, while that of the FL-SOT is of the form, $\vec{\tau}_{FL} = \tau_0^{FL} \vec{m} \times \vec{y}$, which, in contrast to experiment, it does not exhibit higher-order angular terms. We show that both the FL-

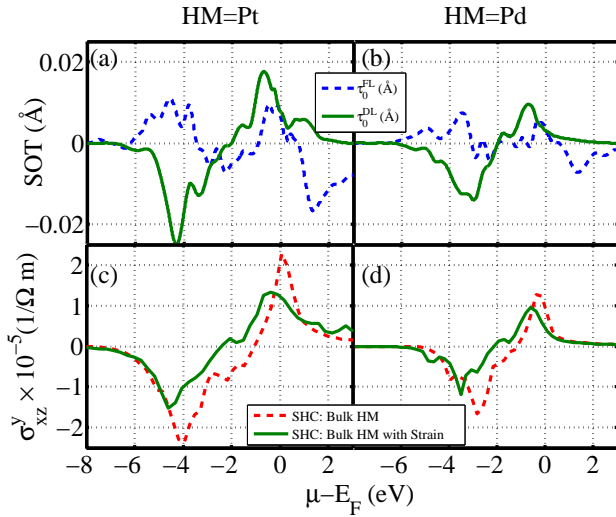


FIG. 6: (Color online) FL- and DL-SOT as a function of Fermi level position for (a) Pt (6 ML)/Co (6 ML) and (b) Pd(6 ML)/Co (6 ML). Spin Hall conductivity, σ_{xz}^y , as a function of Fermi level position for bulk (c) Pt and (d) Pd, under zero and -11% (Pt) and -9% (Pd) compressive biaxial strain which lead to 17%(Pt) and 12%(Pd) increase of the out-of-plane interlayer distance.

and DL-SOTs are dominated by electrons on the Fermi surface. In Pt/Co both components of SOT increase with increasing tensile biaxial strain on Co, while in Pd/Co only the DL-SOT increases under tensile strain. The DL-SOT decreases quadratically with the HM thickness while the FL-SOT saturates to a finite value in Pt/Co while it reverses sign in Pd/Co. The dependence of the SOT with the position of the Fermi level suggests that the DL-SOT results from the Spin Hall effect of the bulk HM.

Acknowledgments

The work is supported by NSF ERC-Translational Applications of Nanoscale Multiferroic Systems (TANMS)-Grant No. 1160504 and by NSF-Partnership in Research and Education in Materials (PREM) Grant No. DMR-1205734.

* Electronic address: Farzad.Mahfouzi@gmail.com

† Electronic address: Nick.Kioussis@csun.edu

¹ A. Manchon and S. Zhang, Theory of nonequilibrium intrinsic spin torque in a single nanomagnet, *Phys. Rev. B* **78**, 212405, (2008).

² Ioan Mihai Miron, Kevin Garello, Gilles Gaudin, Pierre-Jean Zermatten, Marius V. Costache, Stéphane Auffret, Sbastien Bandiera, Bernard Rodmacq, Alain Schuhl and Pietro Gambardella, Perpendicular switching of a single ferromagnetic layer induced by in-plane current injection, *Nature* **476**, 189193 (2011).

³ Luqiao Liu, O. J. Lee, T. J. Gudmundsen, D. C. Ralph, and R. A. Buhrman, Current-Induced Switching of Perpendicularly Magnetized Magnetic Layers Using Spin Torque from the Spin Hall Effect, *Phys. Rev. Lett.* **109**, 096602 (2012).

⁴ L. Liu, C. F. Pai, Y. Li, H. W. Tseng, D. C. Ralph, and R. A. Buhrman, Spin-Torque Switching with the Giant Spin Hall Effect of Tantalum, *Science* **336**, 555 (2012).

⁵ M. Cubukcu, O. Boulle, M. Drouard, K. Garello, C. O. Avci, I. M. Miron, J. Langer, B. Ocker, P. Gambardella, and G. Gaudin, Spin-orbit torque magnetization switching of a three-terminal perpendicular magnetic tunnel junction, *Appl. Phys. Lett.* **104**, 042406 (2014).

⁶ C. Zhang, S. Fukami, H. Sato, F. Matsukura, and H. Ohno, Spin-orbit torque induced magnetization switching in nanoscale Ta/CoFeB/MgO, *Appl. Phys. Lett.* **107**, 012401 (2015).

⁷ Ioan Mihai Miron, Gilles Gaudin, Stéphane Auffret, Bernard Rodmacq, Alain Schuhl, Stefania Pizzini, Jan Vogel and Pietro Gambardella, Current-driven spin torque induced by the Rashba effect in a ferromagnetic metal layer, *Nature Materials* **9**, 230234 (2010).

⁸ K. Garello, I. M. Miron, C. O. Avci, F. Freimuth, Y. Mokrousov, S. Blugel, S. Auffret, O. Boulle, G. Gaudin and P. Gambardella, Symmetry and magnitude of spin-orbit torques in ferromagnetic heterostructures. *Nature Nanotechnology* **8**, 587593 (2013).

⁹ P. M. Haney, H.-W. Lee, K.-J. Lee, A. Manchon, and M. D. Stiles, Current induced torques and interfacial spin-orbit coupling: Semiclassical modeling, *Phys. Rev. B* **87**, 174411 (2013).

¹⁰ Ki-Seung Lee, Dongwook Go, Aurlien Manchon, Paul M. Haney, M. D. Stiles, Hyun-Woo Lee, and Kyung-Jin Lee, Angular dependence of spin-orbit spin-transfer torques, *Phys. Rev. B* **91**, 144401 (2015).

¹¹ F. Freimuth, S. Blgel, and Y. Mokrousov, Spin-orbit torques in Co/Pt (111) and Mn/W (001) magnetic bilayers from first principles, *Phys. Rev. B* **90**, 174423 (2014).

¹² Wei Zhang, Matthias B. Jungfleisch, Frank Freimuth, Wanjun Jiang, Joseph Sklenar, John E. Pearson, John B. Ketterson, Yuriy Mokrousov, and Axel Hoffmann, All-electrical manipulation of magnetization dynamics in a ferromagnet by antiferromagnets with anisotropic spin Hall effects, *Phys. Rev. B* **92**, 144405 (2015).

¹³ Sucheta Mondal, Samiran Choudhury, Neha Jha, Arnab Ganguly, Jaivardhan Sinha, and Anjan Barman All-optical detection of the spin Hall angle in W/CoFeB/SiO₂ heterostructures with varying thickness of the tungsten layer, *Phys. Rev. B* **96**, 054414 (2017).

¹⁴ K. Ando, S. Takahashi, K. Harii, K. Sasage, J. Ieda, S. Maekawa, and E. Saitoh, Electric Manipulation of Spin Relaxation Using the Spin Hall Effect *Phys. Rev. Lett.* **101**, 036601 (2008).

- ¹⁵ Ung Hwan Pi, Kee Won Kim, Ji Young Bae, Sung Chu Lee, Young Jin Cho, Kwang Seok Kim, and Sunae Seo, Tilting of the spin orientation induced by Rashba effect in ferromagnetic metal layer, *Applied Physics Letters* **97**, 162507 (2010).
- ¹⁶ Masamitsu Hayashi, Junyeon Kim, Michihiko Yamanouchi, and Hideo Ohno, Quantitative characterization of the spin-orbit torque using harmonic Hall voltage measurements, *Phys. Rev. B* **89**, 144425 (2014).
- ¹⁷ Abhijit Ghosh, Kevin Garelo, Can Onur Avci, Mihai Gabureac, and Pietro Gambardella, Interface-Enhanced Spin-Orbit Torques and Current-Induced Magnetization Switching of Pd/Co/AlO_x Layers, *Phys. Rev. Applied*, **7**, 014004 (2017).
- ¹⁸ David MacNeill, Gregory M. Stiehl, Marcos H. D. Guimaraes, Neal D. Reynolds, Robert A. Buhrman, and Daniel C. Ralph, Thickness dependence of spin-orbit torques generated by WTe₂, *Phys. Rev. B* **96**, 054450 (2017).
- ¹⁹ Luqiao Liu, Takahiro Moriyama, D. C. Ralph, and R. A. Buhrman, Spin-Torque Ferromagnetic Resonance Induced by the Spin Hall Effect, *Phys. Rev. Lett.* **106**, 036601 (2011).
- ²⁰ A. Kumar, S. Akansel, H. Stopfel, M. Fazlali, J. kerman, R. Brucas, and P. Svedlindh, Spin transfer torque ferromagnetic resonance induced spin pumping in the Fe/Pd bilayer system, *Phys. Rev. B* **95**, 064406, (2017).
- ²¹ A. R. Mellnik, J. S. Lee, A. Richardella, J. L. Grab, P. J. Mintun, M. H. Fischer, A. Vaezi, A. Manchon, E.-A. Kim, N. Samarth and D. C. Ralph, Spin-transfer torque generated by a topological insulator, *Nature* **511**, 449451 (2014).
- ²² A. M. Goncalves, I. Barsukov, Y.-J. Chen, L. Yang, J. A. Katine, and I. N. Krivorotov, Spin torque ferromagnetic resonance with magnetic field modulation *Appl. Phys. Lett.* **103**, 172406 (2013).
- ²³ Xin Fan, Halise Celik, Jun Wu, Chaoying Ni, Kyung-Jin Lee, Virginia O. Lorenz and John Q. Xiao, Quantifying interface and bulk contributions to spinorbit torque in magnetic bilayers, *Nature Communications* **5**, 3042 (2014).
- ²⁴ Xin Fan, Alex R. Mellnik, Wenrui Wang, Neal Reynolds, Tao Wang, Halise Celik, Virginia O. Lorenz, Daniel C. Ralph, and John Q. Xiao, All-optical vector measurement of spin-orbit-induced torques using both polar and quadratic magneto-optic Kerr effects, *Appl. Phys. Lett.* **109**, 122406 (2016).
- ²⁵ Xuepeng Qiu, Praveen Deorani, Kulothungasagaran Narayanapillai, Ki-Seung Lee, Kyung-Jin Lee, Hyun-Woo Lee and Hyunsoo Yang, Angular and temperature dependence of current induced spin-orbit effective fields in Ta/CoFeB/MgO nanowires, *Scientific Reports* **4**, 4491 (2014).
- ²⁶ Junyeon Kim, Jaivardhan Sinha, Masamitsu Hayashi, Michihiko Yamanouchi, Shunsuke Fukami, Tetsuhiro Suzuki, Seiji Mitani and Hideo Ohno, Layer thickness dependence of the current-induced effective field vector in Ta/CoFeB/MgO, *Nature Materials* **12**, 240245 (2013).
- ²⁷ F. Mahfouzi, B. K. Nikolić, and N. Kioussis, Antidamping spin-orbit torque driven by spin-flip reflection mechanism on the surface of a topological insulator: A time-dependent nonequilibrium Green function approach, *Phys. Rev. B* **93**, 115419 (2016).
- ²⁸ L. Wang, R. J. H. Wesselink, Y. Liu, Z. Yuan, K. Xia, and P. J. Kelly, Giant Room Temperature Interface Spin Hall and Inverse Spin Hall Effects, *Phys. Rev. Lett.* **116**, 196602 (2016).
- ²⁹ Minh-Hai Nguyen, D. C. Ralph, and R. A. Buhrman, Spin Torque Study of the Spin Hall Conductivity and Spin Diffusion Length in Platinum Thin Films with Varying Resistivity, *Phys. Rev. Lett.* **116**, 126601 (2016).
- ³⁰ Farzad Mahfouzi. Nonequilibrium Green Function Approach to Elastic and Inelastic Spin-Charge Transport in Topological Insulator-Based Heterostructures and Magnetic Tunnel Junctions. PhD dissertation, University of Delaware. Ann Arbor: ProQuest/UMI. (Publication No. 3642336.).
- ³¹ H. Kurebayashi, Jairo Sinova, D. Fang, A. C. Irvine, T. D. Skinner, J. Wunderlich, V. Novk, R. P. Campion, B. L. Gallagher, E. K. Vehstedt, L. P. Zrbo, K. Vyborny, A. J. Ferguson and T. Jungwirth, An antidamping spinorbit torque originating from the Berry curvature, *Nature Nanotechnology* **9**, 211217 (2014).
- ³² Farzad Mahfouzi, Branislav K. Nikolic, and Nicholas Kioussis, Antidamping spin-orbit torque driven by spin-flip reflection mechanism on the surface of a topological insulator: A time-dependent nonequilibrium Green function approach, *Phys. Rev. B* **93**, 115419 (2016).
- ³³ Farzad Mahfouzi, Branislav K. Nikoli, Son-Hsien Chen, and Ching-Ray Chang, Microwave-driven ferromagnetotopological-insulator heterostructures: The prospect for giant spin battery effect and quantized charge pump devices, *Phys. Rev. B* **82**, 195440 (2010).
- ³⁴ G. Kresse and J. Furthmüller, Efficient iterative schemes for ab initio total-energy calculations using a plane-wave basis set, *Phys. Rev. B* **54**, 11169 (1996).
- ³⁵ G. Kresse and J. Furthmüller, Efficiency of ab-initio total energy calculations for metals and semiconductors using a plane-wave basis set, *Comput. Mater. Sci.* **6**, 15 (1996).
- ³⁶ P. E. Blöchl, Projector augmented-wave method, *Phys. Rev. B* **50**, 17953 (1994).
- ³⁷ G. Kresse and D. Joubert, From ultrasoft pseudopotentials to the projector augmented-wave method, *Phys. Rev. B* **59**, 1758 (1999).
- ³⁸ J. P. Perdew, K. Burke, and M. Ernzerhof, Generalized Gradient Approximation Made Simple, *Phys. Rev. Lett.* **77**, 3865 (1996).
- ³⁹ A. A. Mostofi, J. R. Yates, G. Pizzi, Y.-S. Lee, I. Souza, D. Vanderbilt, and N. Marzari, An updated version of wannier90: A tool for obtaining maximally-localised Wannier functions, *Comput. Phys. Commun.* **185**, 2309 (2014).
- ⁴⁰ Farzad Mahfouzi, Jinwoong Kim, and Nicholas Kioussis, Intrinsic damping phenomena from quantum to classical magnets: An ab initio study of Gilbert damping in a Pt/Co bilayer, *Phys. Rev. B* **96**, 214421 (2017).
- ⁴¹ Yi Liu, Zhe Yuan, R. J. H. Wesselink, Anton A. Starikov, Mark van Schilfgaarde, and Paul J. Kelly, Direct method for calculating temperature-dependent transport properties, *Phys. Rev. B* **91**, 220405(R) (2015).